THE JOURNAL OF PHYSICAL CHEMISTRY A

ARTICLE

pubs.acs.org/JPCA

Effects of Various Boundary Conditions on the Response of Poisson−Nernst−Planck Impedance Spectroscopy Analysis Models and Comparison with a Continuous-Time Random-Walk Model

J. Ross Macdonald*

Department of Physics and Astronomy, University of North Carolina, Chapel Hill, North Carolina 27599, United States

ABSTRACT: Various electrode reaction rate boundary conditions suitable for mean-field Poisson−Nernst−Planck (PNP) mobile charge frequency response continuum models are defined and incorporated in the resulting Chang−Jaffe (CJ) CJPNP model, the ohmic OHPNP one, and a simplified GPNP one in order to generalize from full to partial blocking of mobile charges at the two plane parallel electrodes. Model responses using exact synthetic PNP data involving only mobile negative charges are discussed and compared for a wide range of CJ dimensionless reaction rate values. The CJPNP and OHPNP ones are shown to be fully equivalent, except possibly for the analysis of nanomaterial structures. The dielectric strengths associated with the CJPNP diffuse double layers at the electrodes were found to decrease toward 0 as the reaction rate increased, consistent with fewer blocked charges and more reacting ones. Parameter estimates from GPNP fits of CJPNP data were shown to lead to accurate calculated values of the CJ reaction rate and of some other CJPNP parameters. Best fits of $CaCu_3Ti_4O_{12}$ (CCTO) single-crystal data, an electronic conductor, at 80 and 140 K, required the anomalous diffusion model, CJPNPA, and led to medium-size rate estimates of about 0.12 and 0.03, respectively, as well as good estimates of the values of other important CJPNPA parameters such as the independently verified concentration of neutral dissociable centers. These continuum-fit results were found to be only somewhat comparable to those obtained from a composite continuous-time random-walk hopping/trapping semiuniversal UN model.

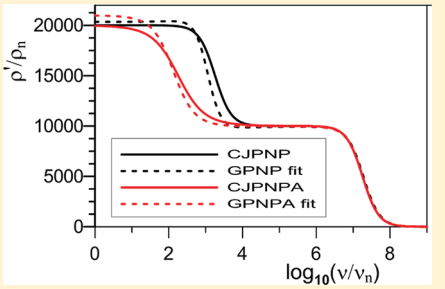

1. INTRODUCTON AND BACKGROUND

Impedance spectroscopy, or more generally, immittance spectroscopy, the analysis of experimental electrical response data in the frequency and/or temporal domain, has proved very powerful in helping to elucidate the various electrical processes present in a material that lead to the observed response. To adequately do so, however, one requires a computer program, such as LEVM,[1] that may be used to fit a given model with the data, preferably using complex nonlinear least squares (CNLS) in the frequency domain. Two quite different general models have seen most use so far and have proved most appropriate, especially for materials containing mobile ions. They are of one-dimensional character and apply to a cell with two identical electrodes. One such model, the Kohlrausch semiuniversal UN one, involves hopping and trapping of mobile charges and is usually based on a continuous-time random-walk (CTRW) procedure.[2−4] Another one, a continuum approach discussed below, considers ordinary or anomalous diffusion and involves a mean-field approximation. They both may be applied with varying success for ionic or electronic conduction in such materials as single-crystal solids, disordered materials such as glasses, some polymers and gels, supercooled liquids, and even photoconductors. Here, we deal with materials exhibiting either ionic or electronic conduction.

Because many experiments involve incompletely blocking electrodes, one needs to consider boundary conditions that range from complete blocking to very rapid electrode reactions, which, in the limit, lead to fully transparent nonblocking behavior. In the present work, we consider the response of the diffusional Poisson−Nernst−Planck (PNP) model for three somewhat different partial-blocking boundary condition expressions and also discuss its relation to an important CTRW model for analyzing conductive systems.

The first PNP impedance response model that properly included satisfaction of the Poisson equation appeared in 1953[5] and involved completely blocking electrodes. In 1954, partial-blocking effects were included by Friauf[6] by using the Chang−Jaffe (CJ) boundary conditions.[7] A more complete CJPNP theoretical model appeared in 1973[8] and a very general one in 1978.[9] In addition, some CJPNP full- and zero-blocking effects were demonstrated earlier in 1971.[10] Generalizations of the fully blocking PNP model to include anomalous diffusion, the PNPA one, appear in refs 11 and 12 and will also be used and extended here to partial-blocking boundary conditions for fitting experimental data involving electrode reactions. Here, using the CJPNP model of ref 9 for only negative charges mobile (the one-mobile case), we first discuss the effects of the CJ boundary conditions and compare the results with those following from two other response models, the GPNP one and an ohmic one, the OHPNP. The CJPNP and GPNP models, and their anomalous diffusion (fractional exponent) generalizations, the CJPNPA

Received: July 14, 2011
Revised: September 16, 2011
Published: September 16, 2011

and GPNPA ones, have been used to fit experimental data in refs 11 and 12 but without explicit comparison of boundary conditions. Ohmic and some other partial-blocking boundary conditions were described in 2005 along with earlier references,[13] and ohmic boundary conditions were used with the PNP equations[5] in 2007 to independently develop the OHPNP model.[14] For simplicity, we shall hereafter take model names such as the CJPNP one to implicitly include the possibility of anomalous diffusion and only refer to names such as the CJPNPA when the distinction between ordinary and anomalous diffusion needs to be made explicit.

Experimental data viewed at the impedance or complex resistivity immittance level often show two real-part plateaus at low and mid frequencies. Although generation−recombination (GR) effects even with completely blocking electrodes can lead to two such plateaus for a limited range of incomplete dissociation of charges,[11] there is still no DC conduction because the real part of the conductivity continually decreases as the frequency decreases toward 0. Further, no separate low-frequency GR plateau appears for either full dissociation or for very small dissociation. Here, therefore, we consider partially blocking electrode situations that do lead to DC conduction and to two plateaus not associated with GR. The two two-plateau situations may be readily distinguished by considering the real-part response of the admittance or conductivity at low frequencies; only for the partial-blocking situation will a low-frequency conductivity plateau appear. We therefore consider here only the partially blocking situation for those small-dissociation GR conditions that do not themselves lead to two plateaus,[11] thus not including three or more possibly distinct plateau situations.[15]

We first summarize impedance-level expressions for the three partial-blocking models. Then, these results are used to obtain the zero-frequency responses of the CJPNP and GPNP models at the impedance and dielectric constant immittance levels. These responses are then used to establish first an exact relation between the GPNP boundary parameter, $G = G_P \equiv 1/R_P$, and the normalized dimensionless CJ reaction rate parameter, ρ_2. Its symbol should not be confused with that for resistivity, and it is used here for historical continuity since its definition in 1973.[8,9] Another important relation is established between ρ_2 and the normalized limiting-low-frequency dielectric constant or dielectric strength. Tabular and graphic comparisons of CJPNP and GPNP exact model responses are followed by a discussion and illustration of the use of the CJPNPA and GPNPA models in fitting and analyzing experimental data sets. Finally, these continuum system results are compared with ones using the important conductive system Scher-Lax CTRW hopping model,[2] extended by the specific choice in it of a stretched exponential correlation function in the temporal domain (see refs 4 and 16 and earlier publications cited therein), and overall Conclusions appear in section 4.

Although we assume here that specific adsorption is absent, eq (B37) in ref 9 shows how ρ_2 may be generalized to the complex form in the presence of such adsorption. Note that the present PNP models, fully or partially blocking, do not include effects arising from the Stern compact layer at the electrode. Such effects are associated with the finite size of mobile ions and those of solution molecules in the case of supported electrolytes, and their size is taken zero here and earlier because the capacitance of the Stern layer is nearly always much greater than that of the diffuse double layer, and its effects are thus negligible in most immittance spectroscopy data. We thus treat a small-signal, unbiased Gouy−Chapman situation here.[13,17,18]

2. BOUNDARY CONDITIONS AND RELATED MODEL EQUATIONS

2.1. Normalization. For simplicity and clarity, it is convenient to express PNP equations and results in terms of normalized dimensionless quantities insofar as practical, as recently demonstrated in refs 11 and 12. Important bulk quantities are the high-frequency-limiting PNP conductance or conductivity quantities, $G_\infty \equiv 1/R_\infty$ or $\sigma_\infty \equiv 1/\rho_\infty$, respectively, applied for raw data or models or for specific data or models, as described in Appendix A.1 of ref 9. They are independent of electrode effects. The normalized total admittance (or conductivity) is $Y_{TN} \equiv Y_T/G_\infty$, and as discussed in refs 9, 11, and 12, it is particularly useful to divide the full response into a normalized low-frequency interface part, $Y_{iN} \equiv Y_i/G_\infty$, and a bulk high-frequency one involving R_∞ in parallel with the high-frequency, mostly dipolar, bulk capacitance $C_\infty \equiv C_g$, leading to the Debye time constant $\tau \equiv \tau_D \equiv R_\infty C_\infty$.

Further, define the normalized frequency parameter $S \equiv i\omega\tau$. Then, as shown for example in eq (24) of ref 9, Y_{TN} and Y_{iN} are connected by $Y_{TN} = S + 1/[1 + 1/Y_{iN}] \equiv 1/Z_{TN}$. Next, define $P_1 \equiv (1 + S) \equiv p_1^2$ and $q_1 \equiv Mp_1$, where the important quantity M is the ratio of one-half of the separation of plane-parallel electrodes, L, and the Debye length, L_D. Then, define the important frequency-dependent diffusional quantity $Q_1 \equiv [\tanh(q_1)]/q_1$, whose zero-frequency value is just $M^{-1}\tanh(M)$, essentially equal to M^{-1} for $M \geq 5$. The high-frequency-limiting dielectric constant is designated ε_∞; therefore, $C_\infty \equiv (A/L)\varepsilon_V\varepsilon_\infty$, where A is the electrode area and ε_V is the permittivity of vacuum. Here, as in most previous theoretical calculations, A is usually taken of unit size. Finally, for fully blocking conditions, set $Z_{TN} \rightarrow Z_{0N}$, $Y_{TN} \rightarrow Y_{0N}$, and so forth. In this case, relevant PNP equations are[12]

$$Z_{0iN} = P_1Q_1/[S(1 - Q_1)] \quad (1)$$

and

$$Z_{0N} = (S + Q_1)/(SP_1) \quad (2)$$

Note especially that dispersive diffusion effects only appear in the above expression for Z_{0N} through the quantity Q_1. When it is 0 or negligible, the response is that of simple undispersed conductive system Debye character.

2.2. Various Diverse Boundary Conditions, the Resulting CJPNP, GPNP, and OHPNP Models, and a CTRW One. *2.2a. Chang−Jaffe, Ohmic, and Other Related Boundary Conditions.* It has long been known that specific adsorption and double-layer structure influence electrode reactions. Further, "Although PNP equations constitute a well-understood and widely accepted approximation, appropriate boundary conditions for them are not so clear...".[13] Here, we summarize some boundary conditions used in the past for PNP and other models to account for Faradaic redox reactions at metal electrodes in the absence of specific adsorption effects. Although double-layer structure is complex and may involve discreteness-of-charge effects and imaging,[19] possible oscillations of potential arising from the finite sizes of permanent dipoles and ions,[20,21] and overscreening effects,[18] they are of negligible importance here.

Although a thorough and valuable summary of earlier work on charge-transfer kinetics for electrochemical PNP models, including inner-layer effects and an important generalization of the Butler−Volmer (BV) equation, appeared in 2009,[22] neither it nor earlier work cited there directly considered impedance

responses for mean-field PNP models such as those in refs 8 and 9 of 1973 and 1978 involving CJ boundary conditions. Further discussion of these boundary conditions and comparison of their small-signal impedance response consequences with those of the BV equation for both unbiased and biased situations appear in ref 23; see especially Figures 5−8 therein. For zero or small DC bias, differences between BV and CJ impedance responses are negligible.

Here, although we are concerned with liquids as well as solids, we ignore Stern inner-layer effects and deal only with the Gouy−Chapman diffuse double layer arising directly from the solution of the two-electrode, one-dimensional PNP equations without finite ion size effects.[5] We nevertheless demonstrate a surprisingly strong influence of CJPNP model partial blocking of mobile ions at the electrodes on the double layer and thus on the dielectric strength associated with such ions. The theoretical results considered here involve small harmonic perturbations around equilibrium in the absence of external DC bias, allowing linearization. They may thus apply well to the results of usual immittance spectroscopy measurements, and an aim of the current analyses is to investigate the utility of the PNP model and its anomalous diffusion extension, the PNPA,[11,12] for fitting such experimental data.

For identical electrodes and only negative charges mobile, we need consider only appropriate boundary conditions at the surface of one of the electrodes. They are then independent of whether charges arrive there by ordinary or by anomalous diffusion, processes that occur in the interface region of the material but ones that do not influence high-frequency-limiting bulk parameters. First, define e as the charge of the proton and take the valence numbers of positive and negative charges to be equal, with that for negative charges denoted by z_2 and taken as unity herein. As usual, in order to obtain linearized impedance response, we divide all potentials, currents, and concentrations into static and small sinusoidal parts, with the applied sinusoidal potential taken to be smaller in magnitude than k_BT/e, and thus neglect higher-order harmonic terms. Here, k_B is the Boltzmann constant. Define N_0 as the static concentration of a neutral entity, such as a molecule, that may dissociate here into an immobile positive species and a mobile negative one whose equilibrium concentration value is $n_e \equiv n_n$. For small dissociation, the magnitude of the sinusoidal quantity n_n is much smaller than that of N_0.

The CJ boundary condition, described and used in refs 6−9, may now be expressed as

$$I_0 = z_2 e k_2 n_0 \tag{3}$$

where I_0 is the sinusoidal current, k_2 is the reaction rate constant of the negative charges, and n_0 is the value at the surface of the electrode of the difference between the concentration there at a given instant and its equilibrium (zero-field) value. It is convenient to replace k_2 by the dimensionless rate parameters ρ_2 or H, where

$$\rho_2 \equiv (L/2D_2)k_2 \equiv (ML_D/D_2)k_2 \equiv MH \tag{4}$$

and D_2 is the diffusion coefficient of the negative charges. We shall use ρ_2 rather than H in the following because then one need not explicitly consider the value of M. Note, however, that ρ_2 is a derived quantity that itself depends on L.

Although ohmic boundary conditions have been considered for many years, their use with the PNP equations probably first occurred in ref 14, a treatment followed here with helpful further input from one of its authors, Professor G. Barbero. For an ohmic boundary condition,[14] we may write

$$I_0 = k_a E_0 \tag{5}$$

where k_a is defined as the conductivity of the interface electrode solution and E_0 is the sinusoidal electric field at the electrode. It is convenient in the following work to use the dimensionless quantity

$$\Omega_C \equiv \omega_C \tau_D \equiv (e\tau_D/\varepsilon_V)k_a \tag{6}$$

in place of k_a. As we shall see, the CJ and ohmic boundary conditions and their resulting PNP equations are closely related, as shown for example in the CJPNP eq (67) of ref 8, where small-signal electrode fields and surface concentrations appear together with $r_n/2 \equiv \rho_2$.

There are no direct boundary conditions specified in the GPNP and CTRW models, but being conductive system analyses, they lead to nonzero values of the DC conductivity, σ_0, and such values will be compared with those following from the CJ and ohmic response models in the next sections. Such comparison allows relations to be established between their DC quantities and the CJ ρ_2 one.

2.2b. CJPNP Model and Its Consequences. The CJPNP model for only negative charged mobile ions follows from the relation $Y_{iNCJ} \equiv Y_{0iN} + \rho_2$. See ref 8 and eq (40) of ref 9, which also includes arbitrary GR. Its fully blocking response is illustrated in ref 11 and involves a complicated expression for Y_{iN}. In unnormalized form, partial blocking here involves the addition of a conductivity $\sigma_\infty\rho_2$ in parallel with the full-blocking interface conductivity expression. Further, it is straightforward to generalize the one-mobile, partial-blocking response from ordinary diffusion to anomalous diffusion, the CJPNPA model, as demonstrated for full-blocking in refs 11 and 12. Its arbitrary blocking expression is instantiated in LEVM for generating or fitting one-mobile data for any degree of charge dissociation, and it is used for the present CJPNP and CJPNPA calculations and comparisons. Although it is too complicated to list here, there is a useful alternative for the CJPNP situation.

As shown in ref 9, the form of the response for a completely blocking and completely dissociated situation with equal mobilities for the positive and negative charges is quite simple. Further, for full or sufficiently small dissociation, where no GR plateau appears, the form of the normalized response equation is the same because then only the values of ρ_∞ and L_D vary with the amount of dissociation and with the value of the mobility ratio, $\Pi_m \equiv \mu_n/\mu_p$, here taken as 10^{40} or greater. Then we find, being careful to avoid division by 0 in the zero limits of the frequency and/or reaction rate, the following CJPNP partial-blocking expression

$$Z_{TNCJ} = [(S + Q_1) + P_1Q_1\rho_2]/[(SP_1) + P_1^2Q_1\rho_2] \tag{7}$$

which properly reduces to the fully blocking result, $Z_{TN} = Z_{0N}$, of eq 2 when the ρ_2 reaction rate is 0. Of course, for small dissociation, we must include in the fitting model a GR parameter, k_{gr}, discussed below, that determines the actual amount of dissociation present. For most solids, full dissociation is physically most unlikely.

The predictions of eq 7 have been found to agree with those following from the exact LEVM model used here to generate and fit one-mobile data. In the zero-frequency limit, eq 7 leads to

$Z_{TNCJ}(0) \equiv \rho_{TNCJ}(0) \equiv \rho_{TNCJ0} = 1 + 1/\rho_2$ for any M value. Although ρ_2 is taken as a real quantity herein, it may be replaced in eqs 4 and 7 by its complex analogue, eq (B38) of ref 9, which includes the possibilities of ordinary electrode reactions, such reactions and specific adsorption, and specific adsorption alone.

In the present situation, different behavior may appear depending on the order in which the frequency, ν, and ρ_2 are set to 0. When the value of ρ_2 goes to 0, at zero frequency, $Z_{TNCJ}(0)$ becomes infinite. However, in actuality, one never experimentally reaches zero frequency, and eq 7 shows that as ρ_2 approaches 0, the increase of $Z_{TNCJ}(\nu)$ above its full-blocking value of 1 occurs at lower and lower frequencies and eventually falls below the available low-frequency experimental boundary, leading effectively to full-blocking behavior, consistent in that limit with an irrelevant parallel resistance of infinite size.

At the dielectric level, now define $\varepsilon'_{CJN}(\nu) \equiv \varepsilon'_{CJ}(\nu)/\varepsilon_\infty$, with $\varepsilon'_{CJ}(0)/\varepsilon_\infty \equiv \varepsilon_{0NCJ}$. Because partial-blocking boundary conditions ($\rho_2 > 0$) affect the interface region and response, they will influence the limiting normalized dielectric strength, $\Delta\varepsilon_{NCJ}(0) \equiv \varepsilon_{0NCJ} - 1$, where for the PNP with full-blocking $\varepsilon_{0N} = M\,\mathrm{ctnh}(M)$. We are particularly interested in the dependence of ε_{0NCJ} on ρ_2. We can show both analytically and numerically using LEVM that for the CJPNP model

$$\varepsilon'_{NCJ}(0) \equiv \varepsilon_{0NCJ} = 1 + [M\,\mathrm{ctnh}(M) - 1]/[1 + \rho_2]^2 \tag{8}$$

a particularly important exact result that clearly reduces properly for ρ_2 equal to 0 or ∞.

The CJPNP and CJPNPA models may be parametrized in various ways; here, the CJPNPA parameters used in the one-mobile LEVM fitting program instantiation are N_0, L, Π_z, Π_m, k_{gr}, ξ, ρ_2, μ_n, ε_∞, and ψ and are expressed in CGS units[11] (see also the LEVM Manual pp 5−15 through 5−19]. Not all of them are always free to vary, as discussed here and in section 3.3. In particular, Π_z and Π_m, the valence number ratio and the mobility ratio, are fixed here at 1 and 10^{45}, respectively. The parameter ξ is held fixed at a very large value, consistent with one-mobile response, and ψ ($0 < \psi \leq 1$) is fixed at 1 for ordinary diffusion. Here, N_0 is the concentration of originally undissociated neutral entities; L is the electrode separation; the *KDL* parameter used in ref 11 is just the log 10 value of the ratio, k_{gr}, of generation to recombination parameters; and μ_n is the mobility of negative charge carriers. It is also of course necessary to specify the absolute temperature, T, but it is not a free parameter of the model. Finally, M, R_∞ or ρ_∞, and the equilibrium charge concentration of negative mobile charges, n_n, are calculated from the other CJPNP parameter fit estimates.

2.2c. OHPNP Model and Its Consequences. For the OHPNP model,[14] the normalized equation analogous to eq 7 is

$$Z_{TNOH} = [(S + Q_1) + \Omega_C(1 - Q_1)]/[(SP_1) + \Omega_C P_1] \tag{9}$$

a result that properly reduces to the full-blocking one when Ω_C is set to 0. Comparison of eqs 7 and 9 shows that they are only consistent when $\Omega_C = \rho_2 P_1 Q_1$, a frequency-dependent quantity, and also $|Q_1| \ll 1$, requiring $M|q_1| \gg 1$. This inequality is most stringent in the zero-frequency limit and then requires that $M \gg 1$. Because this condition is satisfied, however, for virtually all experimental data, except possibly that of nanomaterials where the present one-dimensional geometry may also need to be replaced by a cylindrical or spherical one, the present data fits are here carried out only with the CJPNP or CJPNPA models, and the above expression for Ω_C could be used to calculate OHPNP relevant values if desired.

For nanomaterial impedance data sets with small M values, however, it may be found that in some cases, ohmic boundary conditions will be more appropriate than CJ ones. A short, independent study by G. Barbero and M. Scalerandi that compares frequency responses for CJPNP, GPNP, and OHPNP models without including fits of experimental data has been kindly sent to me by Professor Barbero and is relevant to some of the results presented below in section 3.1. It has been submitted for publication to *Phys. Rev. E*.

2.2d. GPNP Model and Its Consequences. The basic definition of the partial-blocking GPNP model[11,12] may be expressed as $Y_{TNG} \equiv Y_{TN} + G_{PN}$, where $G_{PN} \equiv G_P/G_\infty \equiv 1/R_{PN}$. It therefore differs from the CJPNP model by the appearance of a conductivity or conductance in parallel with the full-blocking response rather than one in parallel with the interface part of the response only. Although it is thus clearly less physically plausible than is the CJPNP model, and as we shall see, although its partial-blocking fits are simpler and yield less information than do CJPNP ones, its fit parameters may be related to some CJPNP ones; therefore, both models are useful. In normalized terms, its response function is

$$Z_{TNG} = (S + Q_1)/[(SP_1) + G_{PN}(S + Q_1)] \tag{10}$$

reducing to a completely blocked response when $G_{PN} = 0$. If we ensure that in the $S \rightarrow 0$ limit, SG_{PN} goes to 0 as $|G_{PN}|$ approaches infinite size, then the resulting limit of Z_{TNG} will be $R_{PN} \rightarrow \infty$, the proper result. As usual, the transformation to anomalous diffusion involves the introduction of fractional frequency response terms in the interface part of the response.[12]

In the work of ref 12, it was stated that setting R_{PN} equal to the CJPNP low-frequency-limiting quantity $Z_{TNCJ}(0) \equiv \rho_{TNCJ}(0) \equiv 1/\sigma_{TNCJ}(0) = 1 + \rho_2^{-1}$ would not only make the equivalent GPNP quantity, $Z_{TNG}(0) \equiv \rho_{TNG}(0) \equiv \rho'_{TNG0}$, agree with the CJPNP value, but it would ensure that GPNP fit results of CJPNP data would yield excellent agreement over the full frequency range. This conclusion was based only on results for $\rho_2 \ll 1$, however, and it has been found, as demonstrated herein, that it begins to fail for $\rho_2 \geq 0.01$.

In its simplest realization, the GPNP, when expressed at the impedance level, involves a midfrequency normalizing resistance parameter, $R_{\infty G}$, and the parameters G_P, τ_D or ε_∞, and M_G, not necessarily equal to the full-blocking M of the CJPNP model. For comparison with the CJPNP, one would fix G_P at the value $G_\infty/[1 + \rho_2^{-1}]$, leading to $R_{0G} = R_\infty(1 + \rho_2^{-1})$, where R_{0G} is the height of the low-frequency plateau and is necessarily equal to that of the CJPNP model when the GPNP is used to fit CJPNP data. In actual practice, the values of the GPNP parameters are taken as free to vary in fits of experimental or of synthetic data calculated from a fit model. Limitations of the GPNP model for fitting exact CJPNP data are illustrated in section 3.1.

2.2e. Composite UN Model and Its Consequences. Much temporal response data for conductive solids have been found to be of stretched exponential character with a β fractional exponent that is restricted to $0 < \beta \leq 1$. Fourier transformation to the frequency domain leads to an impedance spectroscopy model called the K0 model and indirectly to the related K1 model,

Table 1. Comparison of Reaction Rate Effects of Two Boundary Conditions for the PNP Response Model with Only Negative Charges Mobile, the GPNP and CJPNP Ones[a]

GPNP Model Fits of CJPNP Data					CJPNP Model Exact Data Values			
ρ_2	ρ'_{TNG0}	$\rho_{\infty GN}$	M_G/M	ρ_{PN}	ρ'_{TNCJ0}	ρ'_{TNCJ}		ε'_{TNCJ}
					$\nu = 0$	$\nu = 0$	$\nu = \infty$	$\nu = 0$
0 none	1	1	1	0	1	0	1	M
10^{-4}	10^4	1	1	10001	10001	10^{-4}	1	M
0.01	101	1.010	1/1.02	101.04	101	1/101	1	$M/1.02$
0.1	11	1.100	1/1.21	11.005	11	1/11	1	$M/1.21$
0.5	3	1.500	0.4445	3.001	3	1/3	1	$M/2.25$
1	2	2.000	0.2502	2.001	2	1/2	1	$M/4$
2	1.5	3.000	0.1112	1.501	1.5	1/1.5	1	$M/9$
10	1.1	10.95	1/119.5	1.100	1.1	1/1.1	1	$M/120$
25	1.04	25.27	1/672	1.040	1.04	1/1.04	1	$M/633$
100	1.01	87.52	1/5276	1.010	1.01	1/1.01	1	$M/5050$

[a] Results in normalized form are presented for GPNP fits of exact CJPNP specific data. Normalization is denoted with a subscript N. Thus, $\rho'_{TN} \equiv \rho'_T/\rho_\infty$, where the subscript T denotes a total, not interface, quantity, and $1/\rho_\infty \equiv \sigma_\infty$ is the real part of the high-frequency-limiting conductivity. The G of the GPNP model is here a conductivity, $\rho_P \equiv 1/\rho_P$, in parallel with the full complete-blocking PNP response. As shown in the text, for CJ boundary conditions involving the dimensionless reaction rate ρ_2, $\rho'_{TNCJ}(0) \equiv \rho'_{TNCJ0} = (1 + \rho_2^{-1})$, and the same value is then produced for the $\rho'_{TNG}(0) \equiv \rho'_{TNG0}$ quantity of the GPNP model. Here, $\varepsilon_N \equiv \varepsilon'(\nu)/\varepsilon_\infty$, with ε_∞ the high-frequency-limiting bulk dipolar dielectric constant of the material. Although the value of M is for the tabular results, rounded values were calculated with $M = 10^4$, so that to good approximation $\varepsilon'_{NCJ}(0) \cong M_{CJE} = M/(1 + \rho_2)^2$, an effective dielectric strength CJ expression. The unnormalized GPNP fit parameters are $\rho_{\infty G}$, M_G, $\varepsilon_{\infty G}$, and ρ_P All normalized CJPNP and GPNP parameters involve the CJ bulk parameter ρ_∞.

involving exponents β_0 and β_1, respectively. See, for example, refs 3, 4, 16, and 24 and the Website http://jrossmacdonald.com, where virtues of the K1 and of its semiuniversal UN version (β_1 fixed at 1/3) are summarized. Unlike most conductive system models, the CTRW K1 and UN ones lead to a nonzero high-frequency-limiting capacitance whose dielectric constant symbol and definition is $\varepsilon_{C1\infty} \equiv \beta_1^{-1}\Gamma(\beta_1^{-1})\varepsilon_{Ma}$, where Γ is the gamma function, and for the UN model, $\varepsilon_{Ma} \equiv \tau_{UN}/(\rho_{UN}\varepsilon_V)$, and thus $\varepsilon_{C1\infty} \equiv 6\varepsilon_{Ma}$. Here, τ_{UN} is the characteristic relaxation time of the UN model, and ρ_{UN} would be the DC resistivity of the UN if it were alone. Thus, it might be possible to relate ρ_{UN} to the CJPNP boundary condition reaction rate ρ_2. In addition, a separate parallel capacitance, C, is a necessary part of the full K0 and K1 models and represents the primarily dipolar bulk contribution to the high-frequency dielectric constant, ε_∞. Then, the K1 and UN models are designated the CK1 and CUN ones. A particularly important strength of the CUN model with only its three free parameters is that it is found to fit well a variety of experimental data sets for variations in mobile ion concentrations and temperature over wide ranges. In general, no useful closed frequency response expressions for the K0 and K1 models exist, but they may be accurately calculated numerically using the LEVM program.

Some data sets require for good fitting a more complicated composite UN model, and we shall here be particularly concerned with the $[C\{UN \cdot R_\infty\}]\cdot DC$ and $[C\{UN \cdot R_\infty\}]\cdot DB$ ones. The $\cdot$ symbol denotes a series connection; DC designates the Davidson−Cole model,[11] and DB is a Debye model, both defined at the impedance or complex resistivity level. For specific data, as in the UN fits discussed later, the UN directly involves the free parameters ρ_{UN} and τ_{UN}, and β_{1UN} is fixed at 1/3. In addition, the free parameters C and R_∞ of the model lead to $\varepsilon_{\infty UN}$ and $\rho_{\infty UN}$. Those of the DC or DB (the DC with its fractional exponent $\gamma_{DC} = 1$) are designated ρ_{DC}, τ_{DC}, and γ_{DC}.

3. TABULAR, GRAPHICAL, AND FIT COMPARISONS OF MODEL BEHAVIORS

3.1. Tabular and Graphical PNP Comparisons Using Exact Synthetic Model Data. Table 1 contains ρ_2-dependent results for both the GPNP and CJPNP models based on an accurate CJPNP data set. Except for very large or small reaction rates, both a low-frequency $\rho'_{TN}(\nu)$ plateau and a midfrequency one appear, as shown in the following sections graphically and analytically. For the CJPNP model, the table shows the dependence on reaction rate of the low- and high-frequency limits of the normalized data at the resistivity and conductivity levels. In normalized terms, the real part of the resistivity in the midfrequency plateau region is unity for all rates and therefore is not included in the table. Since the high-frequency-limiting dielectric constant, ε_∞, is also independent of ρ_2, its normalized value of unity is also not included in the table. Particularly noteworthy, however, is the decrease in the low-frequency-limiting normalized dielectric constant, $\varepsilon'_{NCJ}(0)$, as the rate increases. It is exactly described by eq 8. Evidently, the dielectric strength decreases to 0 as the reaction rate becomes large and the diffuse layer is progressively diminished, while no such change occurs for the GPNP model when the value of its M parameter is held fixed, which is not the case when fitting the CJ data. Finally, no tabular results are shown for the OHPNP model because they are virtually identical with the CJPNP ones for the $M = 10^4$ value involved in the present comparisons.

The first line in the table, where ρ_2 is 0, is for full blocking and involves no ρ_2 and thus no partial-blocking plateau. As the results in the table show, not all of the GPNP fit results are identical to those for the CJPNP. They are, nevertheless, closely the same for $\rho_2 \leq 0.01$, and such results led the authors of ref 12 to an erroneous identification of their full equality, independent of ρ_2. Particularly interesting is the ρ_2 dependence of the GPNP effective $\rho_{\infty GN}$ parameter, closely described by $(1 + \rho_2)$ for $\rho_2 < 10$.

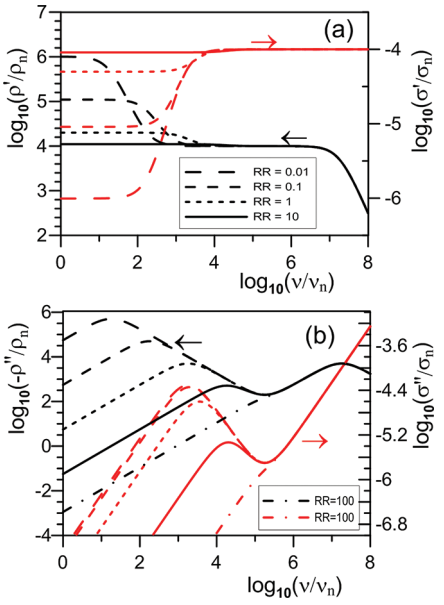

Figure 1. Resistivity (black lines) and conductivity (red lines) CJPNP model exact responses for four different values of the dimensionless reaction rate (RR $\equiv \rho_2$). (a) log−log real parts; (b) log−log imaginary parts. Here and elsewhere, $\rho_n \equiv 1$ ohm−cm; $\sigma_n \equiv 1$ S/cm; and $\nu_n \equiv 1$ Hz.

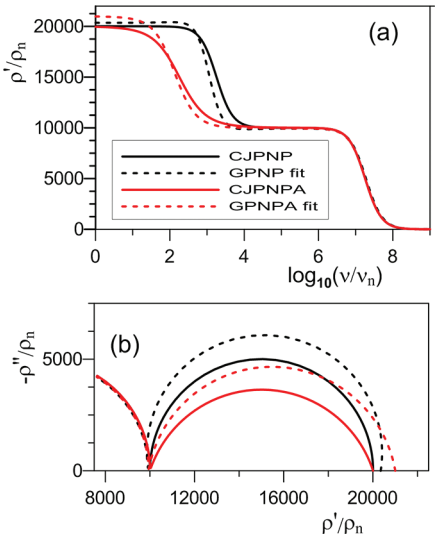

Figure 2. Resistivity-level plots, all derived from exact CJPNP and CJPNPA model data (solid lines) with a dimensionless reaction rate parameter of $\rho_2 = 1$. $\psi = 1$ for the PNP plots and 0.8 for the PNPA ones. Shown are exact CJPNP and CJPNPA responses and GPNP and GPNPA model fits (dashed lines) of their data with M fixed at the CJ full-blocking value of 10^4. (a) Linear log frequency plots and (b) linear−linear resistivity complex plane responses.

Although the normalized midfrequency plateau height, that of ρ_∞, is unity for the exact CJPNP data, its GPNP estimate is clearly appreciably different except in the small reaction rate region.

The GPNP parameter values arising from its fitting of CJPNP data show appreciable similarities with the limiting CJPNP data values. For example, for $\rho_2 \leq 10$, the M_G values are essentially identical to the M_{eff} CJPNP ε'_{NCJNCJ} ones of column 9 of the table. Further, for $\rho_2 < 0.01$, all of the GPNP and CJPNP predictions are virtually identical. The increasing disagreement between the models for $\rho_2 \geq 10$ may arise in part from inaccuracy in the calculations, but it is insignificant because the low-frequency resistivity plateau begins to be indistinguishable from the midfrequency one in this region. The actual relative standard deviations of the GPNP fit residuals, S_F, a measure of goodness-of-fit, varied from about 10^{-8} for very small reaction rates to 10^{-3} for $\rho_2 = 100$. In contrast, fits of experimental data with appropriate models rarely lead to S_F values less than 0.01 or 1%.

Figure 1 compares exact CJPNP reaction rate responses at resistivity and conductivity levels. We see that for RR $\equiv \rho_2 = 10$, the real-part responses are nearly indistinguishable from those of the horizontal midfrequency plateaus. The situation is different, however, for the imaginary-part responses. The left-side resistivity peak keeps increasing as ρ_2 decreases, while the conductivity approaches a limiting response not appreciably different from that shown for $\rho_2 = 0.01$. By the time ρ_2 reaches 100, however, no low-frequency peaks for either resistivity or conductivity remain, and the decreases from the higher-frequency responses continue monotonically on straight lines as the frequency decreases below 10^5 Hz.

Results for the midrange reaction rate value of 1 shown in the table are also presented graphically in Figure 2 and are extended there to show both normal and anomalous diffusion responses. The GPNP fit result of the CJPNP model data for this reaction rate value was indistinguishable from the CJPNP response shown in the figure, and the relative standard deviations of the GPNP parameter estimates were of the order of 10^{-6}; therefore, these fit results are not included here. Instead, the GPNP and GPNPA fit results presented in Figure 2 were carried out with all parameters again free, except for the M one, held fixed at the full-blocking CJPNP value of 10^4, a value following from the CJPNP fit and independent of its ψ and ρ_2 values. When $\psi < 1$, however, there is actually no low-frequency-limiting value of M because then, $\varepsilon(\nu)$ continues to increase as the frequency decreases. Nevertheless, the ψ estimates for the rather poor GPNP and GPNPA fits with the value of M fixed as above were about 1.1 and 0.89, respectively. Because the high-frequency bulk Debye semicircle, which partially appears on the left of Figure 2b, is very nearly independent of ψ and ρ_2 values, most of it is not shown in the figure in order to allow greater resolution of the low-frequency interface responses at the right.

It follows from the table and the above results that the GPNP model may be used with confidence to fit data that might arise from CJ boundary conditions if $\rho_2 \leq 10$ and if it is established that an observed low-frequency $\rho'(\nu)$ plateau arises from DC conduction and not from a complete blocking situation with partial recombination (see ref 11 and earlier references cited therein). Although both processes may lead to two resistance-level plateaus, this recombination situation involves no DC conduction, and thus, no low-frequency-limiting plateau appears in the conductance data.

The GPNP model is appreciably simpler than the CJPNP one, and fits with it yield correspondingly less information because of its fewer parameters than the CJPNP one. It is therefore of interest to discuss what one can learn from a GPNP fit if one assumes that the actual data being fit is best represented by the CJPNP. As the table results show, except for $\rho_2 < 0.01$, GPNP fit estimates of M_G and $R_{\infty G}$ do not represent the full-blocking M and R_∞ CJPNP values well. It is worth emphasizing that the small $\varepsilon'_{NCJ}(0)$ values shown in the last column of the table are not

Table 2. Proportional-Weighting CNLS Fits of CCTO Specific Data Sets at the $\rho(\nu)$ and $\sigma(\nu)$ Immittance Levels[a]

#/ISL, NP	S/P, %	$10^{-20}N_0$, $10^{-12}n_n$ C	ρ_2	μ_n or $10^{-4} \times [\rho_{UN}]$	ε_∞ or $[\varepsilon_{\infty UN}]$	ψ or ψ_G or $[\beta_{1UN}]$	$(10^{-4}\rho_{DC})$ or M C	$(10^6\tau_{DC})$ or $10^{-4}\rho_\infty$	(γ_{DC}) or $(10^{-4}\rho_{\infty G})$	$10^{+6}\sigma_P$ or $[10^{-4}\rho_{\infty UN}]$	M_G or $10^5 \times [\tau_{UN}]$
1/ρ, 35	24, 49	1.07, –	0.105	31.4	72.2	0.831					
2/σ, 35	24, 49	4.10, –	0.102	16.3	88.2	0.873					
3/ρ, 28	16, 33	1.63, –	0.113	23.6	86.0	0.847					
4/σ, 28	15, 31	2.87, –	0.107	18.6	101	0.870					
5/σ_{DC}, 28	3.9, 11	2.38, 4.41	0.062	35.2	117	0.878	(3.32)	(2.05)	(0.772)		
6/ρ, 18	2.9, 6.5	1.84, 3.88	0.114	21.9	174	0.879	359.2	7.360	8.200	1.393	293.3
7/ρ, 18	–, –	1.84 F, 3.88 F	0.114 F	21.9 F	174 F	1 F					
8/ρ_1, 18	16, 23	61.9, 22.5	0.119	3.54	199	1 F					
9/σ, 18	2.4, 5.3	2.38, 4.41	0.114	19.2	171	0.885	386.8	7.376	8.215	1.387	315.8
10/σ, 18	–, –	2.38 F, 4.41 F	0.114 F	19.2 F	171 F	1 F					
11/σ_1, 18	15, 16	68.4, 23.6	0.122	3.62	217	1 F					
12/σ, 23	1.7, 5.6	2.38, 10.42	0.0324	459	174	0.909	445.4	0.1304	0.1346	24.04	419.2
13/σ, 25	3.3, 2.7			[1.366]	[143]	[1/3] F	(2.661)	(637.8)	(1 F)	[0.1300]	[3.16]

[a] Here, ISL designates the immittance spectroscopy level, and NP is the number of data points. All results are for T = 80 K except those of rows 12 ad 13 where T = 140 K. CJPNPA model fit results are in rows 1–4 and 6–12; CJPNPA·DC is in row 5; and $[C\{UN \cdot R_\infty\}] \cdot DB$ is in row 13. Davidson–Cole and Debye parameter symbols are subscripted with DC; GPNPA model parameters involve G and P subscripts and appear in columns 7 and 10–12 of rows 6, 9, and 12. The letter C designates a value calculated from fit parameters, and the letter F indicates that a parameter is fixed for generation of model data or during fitting, as in rows 7, 8, 10, 11, and 13. Percentage values are listed for the goodness-of-fit parameters, $S \equiv S_F$ and $P \equiv$ PDRMS. See section 3.3 for important corrections of some estimates in rows 9 and 12. Parentheses, brackets, and neither are used to distinguish different quantities in the columns.

fitting values but represent the actual effective M values of the data (operationally defined as the ratio of the low-frequency-limiting dielectric constant to the high-frequency-limiting one, ε_∞).

Thus, for $M = 10^4$, for example, the actual low-frequency-limiting dielectric constant predicted from eq 8 of the CJPNP model is only about $1.98\varepsilon_\infty$ for $\rho_2 = 100$, resulting in a dielectric strength parameter value of only $0.98\varepsilon_\infty$. Therefore, even for direct CJPNP fits of appropriate experimental data, it is clear that for $\rho_2 > 0.01$, estimates of the effective M directly from the data will need correction to obtain the value implicit in the model. In this case, however, actual CJPNP LEVM fits, when available, yield a direct estimate of the full-blocking M values as well as those of ρ_2. The decrease in M_{eff} with increasing reaction rate requires a physical explanation, and Dr. F. R. Hamou has plausibly suggested that as larger proportions of the available charge at an electrode react, less remains to contribute to the double-layer capacitance. It is worth noting that in ref 25, the definition of a long-time, mean-square length quantity (their eq 31) related to the displacement of mobile ions involves the dielectric strength parameter and thus the low-frequency-limiting dielectric constant. The analysis involves diffusion of mobile ions, and it seems likely that their results should depend, as in the present eq 8, on electrode reaction rate. Luckily, in many cases, the rate for partially blocking electrodes may be too small to significantly influence their expression.

The present results show that when the underlying data are of CJPNP type, the ratio of the GPNP fit estimate of ρ_P to that of $\rho_{\infty G}$ is just an estimate of ρ_2. One can then use this estimate to obtain an estimate of the CJPNP ρ_∞ quantity from the expressions for either of the above resistivities, an approach likely to be better than a direct estimate from the midfrequency data, because fit estimates are least-squares-averaged quantities. Further, such fit calculations can still yield a useful estimate of ρ_2 even when the data do not extend to low enough frequencies for the limiting-low-frequency plateau to fully appear. Then, for $M \gg 1$, it follows from eq 8 that $M \cong (1 + \rho_2)^2 M_G$, but eq 8 itself should be used for small M. When only GPNP fit estimates are available, It is important to use the corrected M value in calculating the one-mobile Debye length, $L_D \equiv L/2M \equiv [\varepsilon_\infty \varepsilon_V k_B T/(n_n e^2)]^{1/2}$, in order to then obtain an appropriate estimate of n_n.

3.2. Fit Results for Experimental Data. It is difficult to find experimental conductive system data sets whose dimensionless reaction rates are of the order of unity or greater. Some examples of typical $\sigma'(\nu)$ response curves are shown in Figure 1 of ref 26. Many involve a constant plateau at low frequencies, possibly indicating DC behavior, eventually followed by an increasing spur at high frequencies, often with a fractional power law exponent value near 2/3, and some show a decreasing value at sufficiently low frequencies as well, but they rarely include the additional appearance of a very low frequency DC plateau. Wide-range results may also eventually lead, however, to a second (or third) rough plateau in the tera-frequency region [e.g., see ref 27], but here, we consider only two-plateau response up to frequencies of the order of 10^9 Hz or less.

Luckily, appropriate $CaCu_3Ti_4O_{12}$ (CCTO) single-crystal data sets with sputtered gold electrodes exist[28] and have been kindly provided by Dr. P. Lunkenheimer. They show two plateaus up to the GHz region, ones whose heights suggest the possible presence of significant reaction rates. Although their responses were interpreted as possibly involving Schottky diode formation at the electrodes, recent alternate fittings of a 140 K data set with GPNPA and CJPNPA models led to good fits of the data.[12] Although no overt consideration of reaction rates was included there, here, we present further-improved fits of the 140 K set as well as those of an 80 K one, with detailed consideration of the effects of different boundary conditions. It is worth noting that an extension of Schottky barrier theory was presented in 1962,[29]

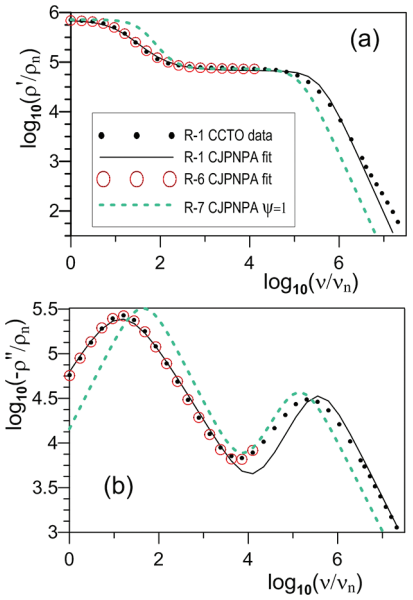

Figure 3. CCTO 80 K data and CJPNPA fits and responses, each designated by row number in Table 2.(a) Log−log real part resistivity data and fits; (b) log−log imaginary part resistivity data and fits.

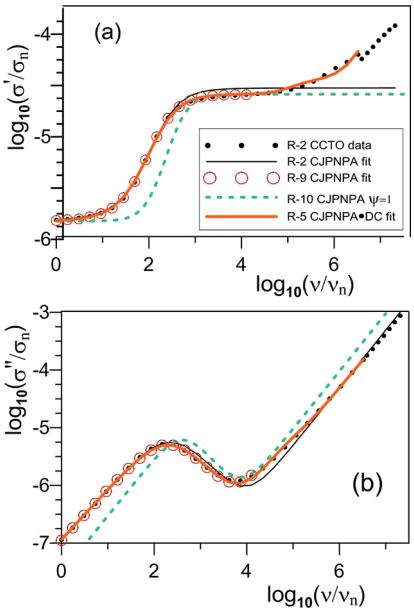

Figure 4. CCTO 80 K data and CJPNPA fits and responses, each designated by row number in Table 2.(a) Log−log real part conductivity data and fits; (b) log−log imaginary -part conductivity data and fits.

but because it involved primarily static current−voltage response but not impedance frequency response, the present CJPNPA theory, which does so, should be more appropriate for zero- or small-bias conditions, as in most small-signal immittance spectroscopy data measurements. Further, the earlier fit of the 140 K data set led to so large an estimate of the mobility of the charges that the conduction process was concluded to be electronic. In this case, of course, the present neglect of inner-layer Stern effects is fully justified.

Fitting of the 80 K set leads to an appreciably larger reaction rate estimate than does the 140 K one; therefore, in Table 2, we first summarize in some detail the steps that led to selection of its best fitting models for the lower-temperature data and present some of the results in Figures 3 and 4. In these figures, results are keyed to appropriate rows in the table; thus R-1 designates the first row of fit estimates. Column 2 of Table 2 includes important S/P goodness-of-fit results, showing values of the relative standard deviation of the fit residuals, S_F, and of PDRMS, the root-mean-square value of the relative standard deviations of the free parameters of the fit, both expressed as percentages, as in ref 12. Excellent fits yield values of these quantities near or less than 1%. The G of the GPNPA model is a conductivity $\sigma_P \equiv 1/\rho_P$.

The parameters of the CJPNPA model are summarized in section 2.2b. Not shown in Table 2 are values of L, the electrode separation, and those of k_{gr}, the ratio of generation to recombination parameters. When N_0 is taken as free to vary during fitting, neither of these two parameters is found to be well determined when also free because LEVM fits show that all three parameters are very highly correlated with each other. However, when N_0 is fixed at its free-fit value, either of the others may be taken as free to vary. We obtained an estimate of 0.297 ± 0.008 cm for L and one of $(8.17 \pm 0.85) \times 10^4$ for k_{gr}, but subsequent important corrections of these results appear in section 3.3. The N_0 and L fit values were found to be temperature-independent. Incidentally, for good fitting of the two-mobile case with mobilities equal to that of the one-mobile one, the L estimate would be twice as large. The (logarithmic) value of KDL of about 4.9 indicates very small dissociation,[11] a result quantified by the estimated values in the table of N_0 and of n_n, the actual concentration of mobile negative charge.

The results of rows 1 and 2 of the table show that the CJPNPA model alone leads to exceptionally poor goodness-of-fit values when fitting the full data set. Although the row 1 ρ' fit shown in Figure 3a appears good up to a frequency of about 3×10^6 Hz, the results in Figure 3b and those shown in Figure 4 still show large discrepancies, and it is evident that a different measuring apparatus was used to obtain results above 3×10^6 Hz than for those at smaller frequencies. Because of this evident mismatch, the fits of rows 3 and 4 were carried out without the top seven data points. As evident, the fits are considerably improved but still very poor. In an effort to account for the remaining spur in $\sigma'(\nu)$, the composite model CJPNPA·DC, involving a Davidson−Cole model in series with the CJPNPA one, was then used; see R-5 in the table and its results shown in Figure 4. The fit is evidently much improved and will be further discussed below.

In R-6 and R-9, CJPNPA and GPNPA fit results, with five free parameters each, are shown for a data set that does not include the right σ' spur shown in Figure 4a, and thus, it extends only to 1.3×10^4 Hz. Although the S_F values are exactly the same for the two models, the PDRMS values are smaller for the GPNPA fits because they do not include the more uncertain N_0 parameter. When it is held fixed, the R-9 PDRMS value reduces to 1.4%, comparable to that for the GPNPA fit of the same data. Comparison of the R-5 and R-9 CJPNPA parameter estimate values shows that not only is the latter fit appreciably better than the former one, but also, its ρ_2, μ_n, and ε_∞ parameter estimates are considerably different and better-determined. Therefore, it is reasonable to conclude that here, the estimates of CJPNPA parameter values from a limited data fit are more appropriate than are those obtained from a particular composite model fit of extended-range data.

In Figures 3 and 4, the results of fitting of the 18-point data sets are shown by open red circles. The closer they each symmetrically encircle a black data point, the better the fit at that frequency. Small discrepancies are evident in the plateau region of Figure 4a, for example, but the agreement is generally good. Note that the agreement between the R-6 and R-9 parameter estimates is also generally good except for the M and M_G parameters, but the conductivity fits are somewhat better than the resistivity ones listed in the table. It follows from the R-6 and R-9 results that the calculation of ρ_2 values from the product $\rho_{\infty G}\sigma_P$ agrees with the CJPNPA estimates to three or more significant figures. Further, the estimation of M from M_G and ρ_2 estimates agrees within about half of the standard deviation of the M_G estimate. Thus, good estimates of relevant CJPNPA parameter values follow here from simpler GPNPA fits.

The fits in R-8 and R-11 of the table are like those of R-6 and R-9, except that the value of ψ was fixed at 1, thus leading to CJPNP rather than CJPNPA fits. We see that the fits and their corresponding parameter estimates are very poor, underlining the need to account for anomalous rather than normal diffusion for this data set. The R-7 and R-10 results shown in the table and in Figures 3 and 4 are not fits but were calculated using the CJPNPA model with all of the parameter estimates of the R-6 and R-9 fits being the same, except with ψ again fixed at 1. The green dashed lines in the figures show the resulting differences between CJPNP and CJPNPA model predictions for these parameter choices.

It is important to compare CCTO data fit results at $T = 80$ and 140 K. The results for the latter in R-12, appreciably improved over the one whose partial results are mentioned in ref 12, should be compared with those in R-9. It is particularly satisfying that the N_0 estimates are the same here and thus temperature-independent within their uncertainties. This is not so, of course, for the k_{gr} and n_n estimates. The R-12 k_{gr} fit estimate was $(4.56 \pm 0.44) \times 10^5$, and it is straightforward to show from the analysis in ref 11 that for small dissociation $n_n \cong [k_{gr}N_0]^{1/2}$, a result fully consistent numerically with the fit results. We expect both n_n and k_{gr} to be thermally activated and thus to trump the effects of just a direct change in temperature. Further, from the definition of M, it follows that one would expect $M_{140}/M_{80} \cong [80(n_n)_{140}/140(n_n)_{80}]^{1/2}$ for temperature-independent ε_∞, again well-satisfied by the present results. Note, however, that these M values both apply for $\psi = 1$.

Next, one can ask whether a CTRW hopping model such as those described in section 2.2e can fit the present 140 K data as well as or better than the continuum CJPNPA one. Upon fitting with the $[C\{UN \cdot R_\infty\}]\cdot$DC model, the S/P values were 3.0 and 2.5, comparable to the corresponding CJPNPA results in R-12 of Table 2, and the γ_{DC} estimate was 0.905, very close to the ψ estimate listed in R-12. Alternately, for the simpler $[C\{UN \cdot R_\infty\}]\cdot$DB model of R-13, the results were 3.3 and 2.7. A very poor fit was obtained, however, with just the $C\{UN \cdot R_\infty\}$ model. For a full composite K1 model fit, the results were 3.3 and 14.4, with the τ_{UN} parameter very poorly estimated and a β_1 estimate of 0.30 ± 0.02. In contrast, a full composite K0 fit led to S/P values of 3.0 and 7.2 and $\beta_0 \cong 0.903$.

Results for the $[C\{UN \cdot R_\infty\}]\cdot$DB model fit with six free parameters are shown in R-13 for comparison with comparable ones in R-12. Clearly, some of the parameters and parameter values in R-13 are related to those in R-12. Both models involve separate ε_∞ parameters, and their estimates are comparable. A crucial difference in their ρ_∞ parameters, however, is that although their estimates are virtually identical, the CJPNPA one of R-12 is an integral part of the model, while the $\rho_{\infty UN}$ one of R-13 is a separate series resistivity, not a direct part of the UN model itself. The presence of such a parameter is further discussed in ref 16, and for both models, its inverse is an estimate of the high-frequency plateau quantity σ_∞.

Finally, the sum of the R-13 ρ_{UN} and ρ_{DC} resistivity values is about 4.03×10^4 ohm−cm, equal to the CJPNPA ρ_∞/ρ_2 value from R-12, the height of the low-frequency plateau above the midfrequency one. Note especially that this boundary value result is here the sum of contributions directly from the UN model and from the Debye one. From its value and the estimated value of the independent series resistivity $\rho_{\infty UN}$, one can immediately obtain an excellent estimate of the CJPNPA electrode reaction rate, however, using only the fit results of the full composite UN model.

At the dielectric level, the $\varepsilon'(\nu)$ data value continually increases as the frequency decreases.[28] This behavior is modeled in the CJPNPA by $\psi < 1$ and partially in the full composite UN model by nearly all of its elements. It is significant that when the parameters of R-13 are used to calculate its response at the dielectric level, the response without $\rho_{\infty UN}$ leads to a low-frequency value of $\varepsilon'(\nu)$ appreciably greater than that of the data. Then, as the frequency increases beyond the UN model characteristic frequency $\nu_{UND} \equiv 1/(2\pi\varepsilon_V\varepsilon_{\infty UN}\rho_{UN})$, approximately 9.2×10^5 Hz here, $\varepsilon'(\nu)$ begins to reach the constant value of 1.57×10^5, that of $\varepsilon_{C1\infty}$ defined in section 2.2e. Most previous UN model fits involved high-resistivity situations where $\varepsilon_{C1\infty}$ was found to be comparable to or smaller in size than $\varepsilon_{\infty UN}$, but here, it is much larger and plays an important role over the full frequency response region. It is significant that anomalous diffusion and composite hopping models can both fit the present limited-range 140 K data set well. This suggests that possibly a combination of the CJPNPA model and a UN one alone might provide a good fit of partial-blocking conductive system data, thus combining the effects of two disparate mobility processes.

It is interesting and significant that when the R-12 CJPNPA fit was used to generate synthetic data from its parameter estimates, the fit of that data using the $[C\{UN \cdot R_\infty\}]\cdot$DB model of R-13 led to S/P values of 2.45 and 3.75%. These values are properly comparable to those listed in R-13 obtained from fitting the original experimental data used in R-12 where the anomalous diffusion parameter estimate was $\psi \cong 0.909$. However, when the R-12 fit parameters with ψ fixed at unity were used to generate exact CJPNP data, its fit using the $[C\{UN \cdot R_\infty\}]\cdot$DB model led to S/P values of 1.4×10^{-6} and 82%, a virtually perfect fit but with the two free ρ_{UN} and τ_{UN} parameters essentially undefined! Thus, in this case, the UN model played no role in the fit, and the Debye part dominated it.

3.3. Consequences of an Incorrect Value of *L*! Since the last section was completed, I learned from the authors of the CCTO work of ref 28 that the actual electrode separation, L, was 1.1 mm rather than about 3 mm, and the area of each electrode was 0.166 cm^2. I have also further investigated the effects of the intercorrelations of the L, k_{gr}, and N_0 CJPNPA parameters. Rather than just replacing the $T = 80$ and 140 K CJPNPA fit results (R-9 and R-12 in Table 2, respectively) and discussion with those for the correct L, taken fixed and temperature-independent here, it is particularly instructive to compare differences in the fit results. It is better to recognize, correct, and learn from errors than just to bury them! First, we find that

the goodness-of-fit values and the figures remain the same, as well as all other parameter estimates, except those of N_0, k_{gr}, n_n, and μ_n.

Unity correlations between fit estimates of N_0 and k_{gr} were avoided by consecutive fits with each parameter separately free to vary until the best-fit combination was found. Although the resulting new CJPNPA model estimate of $N_0 \cong 1.347 \times 10^{22}$ cm^{-3}, the concentration of neutral dissociable entities, was temperature-independent, those of k_{gr} were about 7.69×10^4 and 4.29×10^5 for 80 and 140 K, respectively, not very different from those found for the larger L value. Similarly, the corresponding estimates of n_n and μ_n were 3.22×10^{13} and 7.59×10^{13} cm^{-3} and 2.63 and 63.0 cm^2/(V s), respectively. These mobility estimates are still sufficiently large to rule out ionic conduction.

The large temperature-independent estimate of the concentration N_0 and the small estimates of n_n deserve further physical consideration. Upon being made aware of the present results, Dr. Peter Lunkenheimer, a senior author of ref 28, suggested the following: The edge-length of a cubic unit cell of CCTO is about 7.4×10^{-8} cm,[30] and the cell contains six copper ions, resulting in about 1.48×10^{22} copper atoms per cubic centimeter, close to the independent fit result of $N_0 \cong 1.347 \times 10^{22}$ cm^{-3} and justifying its observed temperature independence.

Because of the high correlations found between N_0 and k_{gr}, their relative estimated standard deviations, even when fitted separately, were each about 10%; thus, the structural value and the present N_0 estimate agree within one standard deviation. Further, when a starting CJPNPA fit with N_0 fixed at 1.48×10^{22} cm^{-3} was carried out using 140 K data, the resulting common estimates of N_0 and k_{gr} were 1.4797×10^{22} and 3.80×10^5 cm^{-3}, respectively, resulting in an unchanged estimate of n_n. Dr. Lunkenheimer has suggested that the very small dissociation found here is likely because the charge carriers are probably associated with small cation nonstoichiometry so that most copper ions provide no mobile electrons. These matters are further discussed in refs 31 and 32.

4. CONCLUSIONS

Comparison of the effects of three different boundary conditions used with the full-blocking PNP ordinary or anomalous diffusion model in order to model partial-blocking nonzero electrode reaction rates shows that the responses of a PNP model with Chang−Jaffe boundary conditions, the CJPNP, and of a PNP model with ohmic boundary conditions, the OHPNP one, are identical for ordinary impedance spectroscopy data. Although the response of the simpler GPNP model with its parameters consistent with those of the CJPNP one only leads to full agreement with that of the CJPNP for very small reaction rates, when the GPNP with free parameters is used to fit CJPNP data, the fit is still nearly exact up to very large rate values. Further, the GPNP fit parameter estimates may be readily transformed to yield the corresponding CJPNP ones without the need for fitting with the more complicated CJPNP model, one which, however, leads to several more important parameter estimates than does the GPNP.

In addition, as the reaction rate increases, the CJPNP model is shown to lead to a progressive decrease in the low-frequency-limiting dielectric constant and thus also in the dielectric strength associated with mobile charge carriers. In the limit of infinite reaction rates, and therefore zero-blocking and transparent electrode behavior, the dielectric strength goes to 0 because all mobile charges at the electrode are then reacting. The above results have been verified by fitting CCTO single-crystal data sets[28] at two different temperatures. They show that the equilibrium concentration of mobile charges is temperature-dependent and very much smaller than the temperature-independent concentration of neutral centers from which they dissociated. Further, this concentration value was shown to agree very closely with one independently derived from the structure of the CCTO material, a further strong verification of the appropriateness of the model. The estimated mobility of the negative charges is so much greater than that expected for ions that these charges are almost certainly electrons arising from nonstoichiometric effects, and the ordinary Gouy−Chapman diffuse layers near the electrodes following from the PNP models seem to lead to results superior to those that invoke possible Schottky barriers at the electrodes.[28]

Finally, it is found that a composite CTRW UN hopping model, the $[C\{\mathrm{UN}\cdot R_\infty\}]\cdot$DB one, fits the present CCTO 140 K data nearly as well as does the continuum CJPNPA model. Although the parameters of the UN model allow it to fit the data in the limited low-frequency range of the CCTO data where some anomalous diffusion increases are present in the low-frequency dielectric constant data, it is found that the $[C\{\mathrm{UN}\cdot R_\infty\}]\cdot$DC model, which involves a fractional exponent in its Davidson−Cole part, leads to a better fit when the data extend to even lower frequencies. It appears, however, that even the series combination of the UN and DC models is unlikely to well fit such anomalous diffusion dielectric behavior if it continues to even lower and lower frequencies. If so, the usual assumption that data arising from continuum and from discrete hopping/trapping processes requires physically different analysis models would be verified.

AUTHOR INFORMATION

Corresponding Author
*E-mail: macd@email.unc.edu.

ACKNOWLEDGMENT

It is a pleasure to thank Professors G. Barbero and M. Z. Bazant and Drs. F. R. Hamou and P. Lunkenheimer, as well as a reviewer, who all provided valuable input and suggestions.

REFERENCES

(1) (a) Macdonald, J. R; Potter, L. D., Jr. *Solid State Ionics* **1987**, *23*, 61–79. (b) Macdonald, J. R. *J. Comput. Phys.* **2000**, *157*, 280–301. The newest WINDOWS version, LEVMW, of the comprehensive LEVM fitting and inversion program may be downloaded at no cost by accessing http://jrossmacdonald.com. It includes an extensive manual and executable and full source code. More information about LEVM is provided at this internet address. All of the J. Ross Macdonald papers cited herein are available in PDF format for downloading from this address.

(2) Scher, H; Lax, M. *Phys. Rev. B* **1973**, *7*, 4491–4519.

(3) Macdonald, J. R. *Phys. Rev. B* **2005**, *71*, 184307/1–184307/12.

(4) Macdonald, J. R. *J. Phys. Chem. Solids* **2009**, *70*, 546–554. The data here were treated as specific but actually were not.

(5) Macdonald, J. R. *Phys. Rev.* **1953**, *92*, 4–17.

(6) Friauf, R. J. *J. Chem. Phys.* **1954**, *22*, 1329–1338.

(7) Chang, H.; Jaffe, G. *J. Chem. Phys.* **1952**, *20*, 1071–1077.

(8) (a) Macdonald, J. R. *J. Chem. Phys.* **1973**, *58*, 4982–5001. (b) Correction: Macdonald, J. R. *J. Chem. Phys.* **1974**, *60*, 343.

(9) Macdonald, J. R.; Franceschetti, D. R. *J. Chem. Phys.* **1978**, *68*, 1614–1637; see also pp 4−9 and 4−10 of the LEVMW manual for discussion of the PNPA model available in the LEVMW fitting program.

(10) Macdonald, J. R. *J. Electroanal. Chem.* **1971**, *32*, 317–328.
(11) Macdonald, J. R. *J. Phys.: Condens. Matter* **2010**, *22*, 495101/1–495101/15. The incorrect eq (A-12) in this work is corrected in Ref 12.
(12) Macdonald, J. R.; Evangelista, L. R.; Lenzi, E. K.; Barbero, G. *J. Phys. Chem. C* **2011**, *115*, 7648–7655.
(13) Bazant, M. Z.; Chu, K. T.; Bayly, B. J. *SIAM J. Appl. Math.* **2005**, *65*, 1463–1484.
(14) Barbero, G.; Batalioto, P.; Figueiredo Neto, A. M. *J. Appl. Phys.* **2007**, *101*, 054102/1–054102/5.
(15) Macdonald, J. R. In *Superionic Conductors*; Mahan, G. D., Roth, W. L., Eds.; Plenum Press: New York, 1976; pp 81−97.
(16) Macdonald, J. R. *Solid State Ionics* **2002**, *150*, 263–279. The symbol $\rho_{C1\infty}$ at the left side of the equation above Figure 6 on p 274 should be replaced by $\tau_{C1\infty}$.
(17) Bazant, M. Z.; Thornton, K; Ajdari, A. *Phys. Rev. E* **2004**, *70*, 021506/1–021506/23.
(18) Bazant, M. Z.; Storey, B. D.; Kornyshev, A. A. *Phys. Rev. Lett.* **2011**, *106*, 046102/1–046102/4.
(19) Barlow, C. A., Jr.; Macdonald, J. R. In *Advances in Electrochemistry and Electrochemical Engineering*; Delahay, P., Ed.; Interscience Publishers: New York, 1967; Vol. VI; pp 1−199.
(20) Macdonald, J. R.; Liu, S. H. *Surf. Sci.* **1983**, *125*, 653–678.
(21) Macdonald, J. R.; Kenkel, S. W. *J. Chem. Phys.* **1984**, *80*, 2168–2182.
(22) Biesheuvel, P. M.; van Soestbergen, M; Bazant, M. Z. *Electrochim. Acta* **2009**, *54*, 4857–4871.
(23) Franceschetti, D. R.; Macdonald, J. R. In *Proceedings of the Third Symposium on Electrode Processes*; Bruckenstein, S. et al., Eds.; The Electrochemical Society: 1980; Vol. 80−3, pp 94−114.
(24) Macdonald, J. R. *J. Phys.: Condens. Matter* **2006**, *18*, 629–644. On p 640, next to the bottom line, replace $\rho_0\varepsilon_{D\infty}$ with $\rho_0\varepsilon_V\varepsilon_{D\infty}$. The word "imaginary" on the third line of p 643 should be replaced by "real.".
(25) Roling, B.; Martiny, C.; Bruckner, S. *Phys. Rev. B* **2001**, *63*, 214203/1–214203/9.
(26) Macdonald, J. R.; Ahmad, M. M. *J. Phys.: Condens. Matter* **2007**, *19*, 046215/1–064215/13.
(27) Kant, Ch.; Rudolf, T.; Mayr, F.; Krohns, S.; Lunkenheimer, P.; Ebbinghaus, S. G.; Loidl, A. *Phys. Rev. B* **2008**, *77*, 045131/1–045131/7.
(28) Krohns, S.; Lunkenheimer, P.; Ebbinghaus, S. G.; Loidl, A. *Appl. Phys. Lett.* **2007**, *91*, 022910/1–022910/3.
(29) Macdonald, J. R. *Solid-State Electron.* **1962**, *5*, 11–37.
(30) Subramanian, M. A.; Li, D.; Duan, N.; Reisner, B. A.; Sleight, A. W. *J. Solid State. Chem.* **2000**, *151*, 323–325.
(31) Li, M; Feteira, A; Sinclair, D. C.; West, A. R. *Appl. Phys. Lett.* **2006**, *88*, 232903/1–232903/3.
(32) Krohns, S.; Lu, J.; Lunkenheimer, P.; Brizé, V.; Autret-Lambert, C.; Gervais, M.; Gervais, F.; Bourée, F.; Porcher, F.; Loidl, A. *Eur. Phys. J. B* **2009**, *72*, 173–182.